Saharan dust intrusions in the Mediterranean area: Three years of Raman lidar measurements

Lucia Mona,[1] Aldo Amodeo,[1] Marco Pandolfi,[1] and Gelsomina Pappalardo[1]

Received 5 August 2005; revised 31 January 2006; accepted 10 May 2006; published 18 August 2006.

[1] A multiyear climatological study of Saharan dust intrusions in the central Mediterranean in terms of aerosol optical parameters vertical profiles is carried out for the first time. Observations are performed at Istituto di Metodologie per l'Analisi Ambientale (IMAA) Raman/elastic lidar station located in Tito Scalo, Potenza (40°36′N, 15°44′E), from May 2000 to April 2003, in the framework of European Aerosol Research Lidar Network (EARLINET). Desert dust aerosols are observed between 1.8 and 9 km in 112 days. Mean values within the desert dust layer of 76 Mm^{-1}, 1.0 Mm^{-1} sr^{-1} and 0.54 Mm^{-1} sr^{-1} are observed for aerosol extinction at 355 nm and aerosol backscatter at 355 and 532 nm. Desert dust layer optical depth at 355 nm ranges between 0.001 and 0.68, with a mean of 0.13. The source origin is the central Sahara in about 65% of the cases, the western Sahara in about 31%, and only in four cases the eastern Sahara. The most extended database of Saharan dust lidar ratio data was collected: Values range between 6 and 126 sr following a 3-modal Gaussian distribution centered at 22, 37 and 57 sr. A mean value of 37 sr is found around the center of the Saharan dust layer. At its extremes, where dust particles are mixed to PBL and free troposphere background aerosols, a mean value of 57 sr is found. Finally, low lidar ratio values of about 22 sr are observed when large amount of dust is transported at low altitudes over the Mediterranean Sea.

Citation: Mona, L., A. Amodeo, M. Pandolfi, and G. Pappalardo (2006), Saharan dust intrusions in the Mediterranean area: Three years of Raman lidar measurements, *J. Geophys. Res.*, *111*, D16203, doi:10.1029/2005JD006569.

1. Introduction

[2] Aerosols play an important role in the atmospheric radiation budget, in fact, depending on the aerosol type, they can absorb or scatter the incoming and outgoing radiation, warming or cooling the atmosphere and, depending on their size and composition, they can act as condensation nuclei, modifying cloud physical and radiative properties [*Kaufman et al.*, 2002]. While it is shown that aerosol clouds injected in the stratosphere by large volcanic eruptions produce a cooling at the surface and an heating of the stratosphere [*Robock*, 2000], the effects of tropospheric aerosols are not yet clear. In fact, tropospheric aerosols are one of the most uncertain elements in the estimation of radiation budget because concentration, shape, size distribution, refractive index and vertical distribution of the tropospheric aerosols, and also the complex mechanisms in which are involved, are highly variable both in time and space [*Intergovernmental Panel on Climate Change* (*IPCC*), 2001]. The continuous soil erosion produces the largest fraction of dust on a global scale, dust that can be transported on long distances by strong winds and convective processes [*d'Almeida et al.*, 1991]. Because dust is a mixture of various minerals, and physical and chemical transformations occur during the transport, the influence of mineral aerosols on radiative forcing is affected by a wide range of uncertainties [*Sokolik and Toon*, 1996]. The main sources of dust are the arid region of the Earth like the Sahara desert and desert areas of Saudi Arabian and eastern Asia. Desert dust constitutes about 40% of aerosol mass yearly injected into the troposphere [*Andreae*, 1995]. One half of this amount is ascribed to the Sahara desert, that with an emission of about 600 Mt per year [*Marticorena and Bergametti*, 1996], is the main localized source region of atmospheric aerosols. Dust particles, lifted by outbreaks in the Sahara region, can travel also on very long distances crossing the North Atlantic Ocean and reaching the southeastern United States [*Prospero*, 1999; *Prospero et al.*, 2002].

[3] A large amount of Saharan dust is transported over the Mediterranean mainly because of cyclone activity inside and around all the area [*La Fontaine et al.*, 1990]. This region is of great interest because several studies indicate that the aerosol radiative forcing over the Mediterranean region is among the highest in the world [*IPCC*, 2001; *Lelieveld et al.*, 2002]. Besides natural desert dust emitted in the Sahara region, different types of aerosol are present in the Mediterranean Basin atmosphere: anthropogenic aerosols produced by urban and industrial areas in continental and eastern Europe; biomass burning aerosols produced in forest fires that often occur during summer; and of course maritime aerosol produced over the Mediterranean sea itself. Moreover, long-range transported aerosols coming

[1]Istituto di Metodologie per l'Analisi Ambientale, Consiglio Nazionale delle Ricerche, Tito Scalo, Italy.

0148-0227/06/2005JD006569

from Asia and North America are observed in the Mediterranean Basin middle troposphere [*Lelieveld et al.*, 2002]. In this complex scheme, Saharan dust intrusion can modify temperature, dynamics and chemical composition of the atmosphere by means of heterogeneous reactions; the deposition of these particles influences biochemical cycles of both aquatic and terrestrial ecosystems [*Lundholm*, 1979]. In addition, mineral aerosols interact with liquid clouds by suppressing precipitation [*Rosenfeld*, 2000] and changing the ice content of clouds [*Pruppacher and Klett*, 1997; *Sassen et al.*, 2003]. Moreover, in the Mediterranean Basin a negative correlation between the desert dust optical depth and the ozone concentration is observed, as a result of the transport of air masses, coming from subtropical area, typically rich in desert dust and contemporary poor in ozone [*di Sarra et al.*, 2002].

[4] Multiyear measurements of the Saharan dust intrusion over Mediterranean area are provided by passive satellite-borne sensors [*Moulin et al.*, 1997; *Husar et al.*, 1997; *Herman et al.*, 1997; *Dulac et al.*, 1992], and ground-based Sunphotometers [*Holben et al.*, 1998]. However, only active techniques, and lidar in particular, allow to distinguish optical effects of local aerosol and lofted plumes and a quantitative description of optical properties of dust complex multilayered structures. This information can be very useful in a complementary approach with column-integrated observations and for aerosol retrieval from satellite measurements. For example, a sensitivity analysis shows that aerosol index provided by the Total Ozone Mapping Spectrometer (TOMS) depends on optical depth, but also that it is related to the aerosol type and altitude [*Hsu et al.*, 1999]. At present, a quantitative equation relating aerosol index to optical depth is available only for desert dust source regions [*Ginoux and Torres*, 2003]. A climatology of desert dust vertical profiles distributed on a continental scale is needed to extend this kind of analysis to other regions.

[5] Among lidar techniques, the Raman/elastic combined approach is the most useful for quantitative studies of tropospheric aerosol. It allows to obtain direct measurement of the ratio between aerosol extinction and backscatter coefficient, i.e., the lidar ratio. This parameter does not depend on the quantity of aerosol, but only on microphysical properties, such as the aerosol size distribution, refractive index, chemical composition and shape [*Evans*, 1988; *Mishchenko et al.*, 1997; *Ackermann*, 1998]. Therefore lidar ratio measurements are a powerful tool in the identification of the kind of aerosol and its properties, especially in the case of tropospheric aerosol layers well separated from the planetary boundary layer [*Mattis et al.*, 2003; *Murayama et al.*, 2004; *Pappalardo et al.*, 2004c].

[6] A main cause of the actual large uncertainties in the estimation of climate forcing by atmospheric aerosols is the limited data on dust climatology [*Sokolik et al.*, 2001]. At present, there are few papers concerning the desert dust vertical distribution over the Mediterranean Basin, typically based on nonsystematic measurements [e.g., *di Sarra et al.*, 2002; *Pace et al.*, 2005; *Formenti et al.*, 2001]. The Saharan dust transport across Europe is continuously monitored since May 2000, within the European Aerosol Research Lidar Network (EARLINET) [*Bösenberg et al.*, 2003], with coordinated measurements at 21 lidar stations distributed around Europe. Systematic lidar observations performed within EARLINET have allowed the collection of a significant database of vertical profiles of Saharan dust optical properties. Within EARLINET, a typical dust outbreak over the eastern Mediterranean [*Papayannis et al.*, 2005], a particular case of long-range transport of Saharan dust to northern Europe [*Ansmann et al.*, 2003], and optical properties of Saharan dust detected during 1 year in the eastern Mediterranean area [*Balis et al.*, 2004] have been analyzed in detail. In addition, a statistical analysis of the occurrences of Saharan dust intrusion over Europe has been carried out [*Papayannis et al.*, 2004].

[7] In this paper, we present results of a climatological study of Saharan dust intrusions in the free troposphere based on measurements performed at IMAA (Istituto di Metodologie per l'Analisi Ambientale) Raman/elastic lidar station located in Tito Scalo, Potenza, during the period May 2000 to April 2003, in the framework of EARLINET. At present, this is the first study on long-term observations of Saharan dust in the central Mediterranean region and the longest climatology of optical properties vertical profiles of Saharan dust. In section 2, we briefly describe the lidar system. The occurrences of Saharan dust observations at our site and its seasonal behavior are discussed in section 3. Then, results concerning altitude range of detected desert dust layer is presented in section 4, where particular attention is devoted to the mixing between the local planetary boundary layer and the desert dust layer itself. Section 5 focuses on the optical properties in the desert dust layer, their seasonal behavior and the comparison with values reported in literature. The identification of the main source regions of Saharan dust and their correlation with the observed optical properties are reported in section 6. Furthermore, section 7 presents a more detailed analysis of lidar ratio database collected within the desert dust layers during these 3 years of measurements, based mainly on the study of lidar ratio values distribution. Finally, a summary of results and conclusions are given in section 8.

2. IMAA Lidar System

[8] The lidar system for tropospheric aerosol study, located at IMAA in Tito Scalo, Potenza (40°36′N, 15°44′E, 760 m above sea level), is a Raman/elastic lidar system operational since May 2000 in the framework of EARLINET, the first lidar network for tropospheric aerosol study on continental scale [*Bösenberg et al.*, 2003]. This system [*Pappalardo et al.*, 2003] is based on a Nd:YAG laser equipped with second and third harmonic generators. Radiation at 355 and 532 nm is transmitted in a coaxial mode into the atmosphere. Elastically backscatter signals at both 355 and 532 nm and N_2 Raman shifted signal are collected with a Cassegrain telescope with primary mirror diameter of 0.5 m and a combined focal length of 5 m. The spectral selection is provided by means of dichroic mirrors and interferential filters with a bandwidth of 1 nm and 0.5 nm, respectively for elastic and Raman channels. For each detected wavelength, the signal is acquired both in analog and photon counting mode. Raw lidar signals have a vertical and temporal resolution of 15 m and 1 minute, corresponding to 1200 laser shots for the pulse repetition rate of 20 Hz typically used.

[9] The combined Raman/elastic approach allows independent measurements of the aerosol extinction and backscatter coefficients [*Ansmann et al.*, 1990; *Ferrare et al.*, 1998]. The aerosol extinction coefficient at 355 nm is retrieved from the nitrogen Raman shifted signal at 386 nm [*Ansmann et al.*, 1990, 1992]. With this information, the only unknown of the elastic lidar equation at 355 nm is the aerosol backscatter coefficient at 355 nm, that is therefore retrievable from the lidar equation without a priori assumption. In this way, the lidar ratio (*LR*) at 355 nm, i.e., the ratio between the aerosol extinction coefficient and the aerosol backscatter coefficient at the same wavelength, is directly obtained. The lidar ratio is an important optical parameter in aerosol characterization, because it depends only on intensive aerosol properties such as chemical composition, size distribution of the particles, and particle shape [*Evans*, 1988; *Mishchenko et al.*, 1997; *Ackermann*, 1998].

[10] The aerosol backscatter coefficient at 532 nm is retrieved with an iterative approach starting from the elastically backscattered lidar signal at this wavelength and assuming a lidar ratio profile at 532 nm. In particular, within Saharan dust layers the mean *LR* at 355 nm calculated in the desert dust layer is rescaled at 532 nm on the basis of values reported in the literature [*Ackermann*, 1998; *Sasano and Browell*, 1989]. For the PBL, a mean *LR* value at 532 nm is assumed on the basis of values reported in the literature [*Ackermann*, 1998; *Sasano and Browell*, 1989] and with the support of multiyear lidar ratio measurements at 355 nm performed at our site [*Pappalardo et al.*, 2004b].

[11] An estimation of the backscatter Ångström exponent or color index can be retrieved from the aerosol backscatter coefficient profiles at 355 and 532 nm assuming a power law wavelength dependence of the aerosol backscatter coefficient. This parameter primarily depends on the size of the particles, assuming lower values for larger particles. A minimum of two aerosol extinction coefficient profiles and three aerosol backscatter coefficient profiles at suitable wavelengths are needed to retrieve information about the aerosol size distribution and chemical composition in a quantitative way [*Müller et al.*, 2001; *Veselovskii et al.*, 2002]. However, lidar ratio measurements at 355 nm together with backscatter measurements at 355 and 532 nm provide qualitative information on the size/composition characteristics of the particles [*Sasano and Browell*, 1989; *Pappalardo et al.*, 2004c].

[12] IMAA Raman/elastic lidar system allows the determination of aerosol optical properties from the lower troposphere up to the upper free troposphere. For low altitudes, it should be considered that the full overlap between the transmitted laser beam and the telescope field of view is reached at about 0.8 km above the lidar station. However, a correction can be introduced in the incomplete overlap region, determining the overlap function [*Wandinger and Ansmann*, 2002]. Since the determination of the aerosol backscatter coefficient profile at 355 nm involves the ratio of lidar signals at 355 and 386 nm, overlap correction is not needed in this case. Typical profiles of the aerosol extinction coefficient at 355 nm and of the aerosol backscatter coefficient at 532 nm start from 500 m above the lidar station. The aerosol backscatter coefficient profiles at 355 nm, instead, typically starts from 400 m above the ground.

[13] Aerosol optical properties vertical profiles are typically obtained with 30 min of temporal integration, and with a vertical resolution of 60 m for the aerosol backscatter coefficient and ranging between 60 and 240 m for the aerosol extinction coefficient.

[14] The systematic errors due to uncertainties in the atmospheric input parameters are of about 10% and 5–10% for the aerosol extinction and backscatter respectively in the PBL [*Ansmann et al.*, 1992, 2002; *Whiteman*, 2003a, 2003b]. Colocated radiosonde profiles are used, when available, to reduce these errors to about 1–5% [*Ansmann et al.*, 1992; *Ferrare et al.*, 1998].

[15] In nighttime conditions, typical statistical errors due to the signals detection are below 5% and 10% in the PBL for the aerosol backscatter coefficients at 355 and 532 nm, and extinction coefficient at 355 nm respectively. In the free troposphere, typical aerosol backscatter coefficient errors are below 30% for values higher than about 0.1 Mm^{-1} sr^{-1} at 355 nm and about 0.07 Mm^{-1} sr^{-1} at 532 nm. For aerosol extinction coefficient, errors are below 30% in the free troposphere for values higher than about 5 Mm^{-1}.

[16] In daytime conditions, the total errors (statistical and systematic) within the PBL are below 15–20% for the aerosol backscatter coefficients at 355 and 532 nm and below 30% for aerosol extinction coefficients. Errors remains below 30% in daytime conditions for aerosol backscatter coefficient values at 355 nm and 532 nm higher than about 0.2 Mm^{-1} sr^{-1} and about 0.1–0.2 Mm^{-1} sr^{-1}, respectively. In daytime conditions, the aerosol extinction coefficient in the free troposphere can be retrieved only if an integration time of 1–1.5 hours is used. In these cases, the total error is lower than 40% for values higher than 80 Mm^{-1}.

[17] The IMAA aerosol lidar system and the algorithms for the aerosol optical parameters retrieval have been successfully tested with different intercomparison exercises in the frame of the EARLINET quality assurance program [*Böckmann et al.*, 2004; *Matthias et al.*, 2004a; *Pappalardo et al.*, 2004a]. These exercises assure that we provide, in the PBL and in free troposphere, high quality profiles of aerosol extinction coefficient at 355 nm, aerosol backscatter coefficient at 355 and 532 nm, and lidar ratio at 355 nm.

[18] Since May 2000, following the EARLINET protocol, we perform regular measurements three times per week: one around noon, when the PBL is well developed, and two within a time window of 1 hour before and up to 3 hours after the sunset. For the retrieval of the aerosol optical properties, signals that indicate the presence of water and ice clouds are removed. Sometimes, especially during winter, weather conditions do not permit lidar operation. Nevertheless, in the May 2000 to April 2003 period we collected lidar measurements for more than 75% of the scheduled EARLINET regular measurements. This large collected data set allowed a characterization of the aerosol typically present over our site [*Matthias et al.*, 2004b; *Pandolfi et al.*, 2004]. Moreover, an alerting system is established within EARLINET in order to perform special measurement campaigns devoted to investigate particular events, like dust intrusions, volcanic eruptions and forest fires [*Ansmann et al.*, 2003; *Pappalardo et al.*, 2004c; *Mattis et al.*, 2003]. Particular attention is devoted to Saharan dust intrusions in Europe, and Saharan dust fore-

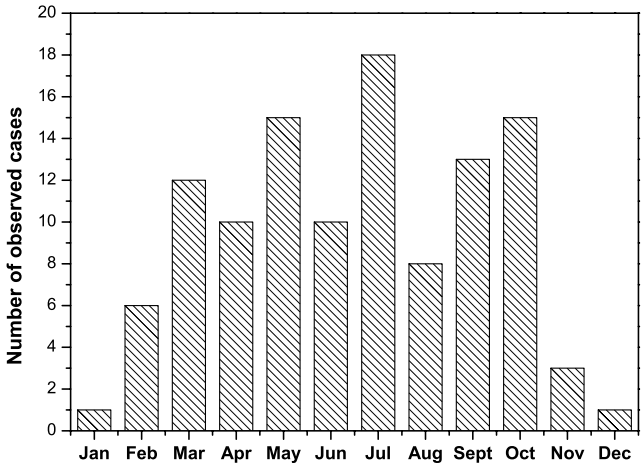

Figure 1. Number of days per month in which Saharan dust intrusions have been observed at IMAA during 3 years of lidar measurements (May 2000 to April 2003).

casts are distributed to all EARLINET stations by the Atmospheric Modeling Weather Forecasting Group of the Athens University, Greece, and by the Euro-Mediterranean Centre on Insular Coastal Dynamics (ICoD).

3. Occurrences

[19] In the period May 2000 to April 2003, we collected more than 1200 hours of lidar measurements (both routine and special measurements) for a total amount of 600 profiles of aerosol optical properties stored in the EARLINET database. A set of criteria is applied to identify, among all measurements (routine and special), the cases with Saharan dust intrusion at our site.

[20] First of all, data characterized by the presence of an aerosol layer above the retrieved PBL [*Matthias et al.*, 2004b] are selected. Among these cases, we consider only those for which the observed aerosol layer is originated in the Sahara region. To identify the origin of the observed aerosol layer, the 4-day backward trajectories provided by the German Weather Service (DWD) are utilized. The DWD provides these back trajectories at each EARLINET lidar station for two arrival times per day and for six arrival pressure levels between 200 and 975 hPa [*Bösenberg et al.*, 2003]. Particle position error is about 10–20% of the trajectory length, with lower uncertainty for higher wind speed [*Stohl*, 1998]. Because of the low error, these trajectories are commonly and efficiently used to identify the pathway and origin of aerosol, pollutant and atmospheric tracers [*Stohl*, 1998]. For each case of aerosol layer observed above the PBL, we studied the pathway and origin of air masses reaching Potenza at the altitude range where the aerosol layer is observed. Only the cases with air masses clearly coming from the Sahara region are considered.

[21] Finally, we have to identify the cases in which air masses coming from the Sahara region carry on lofted desert dust particles. For this aim, images of Aerosol Index provided by TOMS are utilized. These images show if there is a Saharan dust outbreak in correspondence of the back trajectory coming from Sahara and reaching Potenza at altitudes where aerosol layer is observed. For the study of Saharan dust intrusions, we consider only cases in which all the following requirements are satisfied: (1) An aerosol layer above the PBL is observed, (2) the back trajectories analysis show air masses coming from Sahara region, and (3) air masses come from the surface of the Sahara region or TOMS images show a Saharan dust outbreak.

[22] In this way, over 3 years of regular and special measurements we identify aerosol layers related to Saharan dust outbreaks in 112 days. For these Saharan dust measurements, we have an amount of 108 and 91 aerosol backscatter coefficient profiles at 532 and 355 nm respectively, and 52 profiles of the aerosol extinction coefficient and lidar ratio at 355 nm. The relative lower number of extinction profiles is due to the low signal-to-noise ratio of the nitrogen Raman signal in daytime conditions that often does not allow to retrieve the aerosol extinction profile in the free troposphere. The high occurrence of Saharan dust intrusion, corresponding to about 1 day of intrusion every 10 days, is mainly caused by the short distance between our site and the different source regions in the Sahara desert. In particular, a large number of Saharan dust observations are collected in the May–July period (Figure 1), and two relative maxima are observed in March and October. The low number of Saharan dust intrusions observed during winter can be related to the low dust emission typical of this period [*Marticorena et al.*, 1997; *d'Almeida*, 1986], and to the strong seasonal behavior of the dust transport in the Mediterranean area [*Prospero et al.*, 2002; *Moulin et al.*, 1998].

4. Altitude Range

[23] Lidar technique can provide a characterization in terms of the top, base and center of mass of the desert dust layer. For each day of observation, the vertical structure of the desert dust layer is determined from the aerosol backscatter profile (β). In particular, the altitude of the base of the aerosol layer z_b corresponds to the lowest point, over the retrieved PBL [*Matthias et al.*, 2004b], of a strong increase in the backscatter profile. When Saharan dust intrusion in the PBL is observed, the top of the PBL itself has been considered as the base of the desert dust layer in the free troposphere. The top of the desert dust layer is located at the altitude z_t at which both the aerosol backscatter and its first derivative become zero within the experimental error. In some cases, the aerosol vertical structure is very complicated because desert dust layers are present at different altitudes: For these cases a total layer resulting from the multilayered structure is considered for the calculation of mean optical parameters and integrated values.

[24] Table 1 reports mean, minimum and maximum values of desert dust altitude range parameters. As shown in Table 1, experimental distribution of all these parameters is well fitted by a Gaussian distribution (correlation coefficient r higher than 0.9) centered around the experimental mean value. On average the observed desert dust layer extends between 2.5 and 5.9 km above sea level (a.s.l.), reaching a maximum altitude of about 9 km and a minimum one of about 1.8 km (see Table 1). The desert dust particles are often spread on an altitude range of about 3.4 km. This wide altitude range is mainly due to our site proximity to the source region, and to the strong convective regimes that

Table 1. Altitude Range of Desert Dust Layers Retrieved Starting From the Aerosol Backscatter Profile at 532 nm[a]

Layer Part	Mean, km	Minimum, km	Maximum, km	Gaussian Fit M, km	Gaussian Fit Σ, km	Gaussian Fit *r*
Base	2.5 ± 0.5	1.75	6.1	2.3	0.6	0.98
Top	5.9 ± 1.2	3.1	8.9	5.8	2.6	0.94
Thickness	3.4 ± 1.3	8.5	6.9	3.3	2.6	0.93
Center of mass	3.5 ± 0.6	2.3	6.6	3.5	1.1	0.99

[a]For each quantity the mean (μ), the standard deviation (σ) and the correlation coefficient (*r*) of the Gaussian fitting curve are also reported.

typically develop over the Sahara desert. This also explains the elevated altitudes reached by the dust at our site. The proximity of the dust source causes many intrusions of desert dust particles below 2.5 km. This altitude is very close to the local PBL top height that typically ranges between 2 and 2.6 km a.s.l. in nighttime conditions [*Pandolfi et al.*, 2004; *Matthias et al.*, 2004b], indication that sometimes desert dust can be detected also in the local PBL.

[25] For each day of dust observation, we calculate also the backscatter weighted altitude z_c as follows:

$$z_c = \frac{\int_{z_b}^{z_t} z \cdot \beta(z) \cdot dz}{\int_{z_b}^{z_t} \beta(z) \cdot dz} \quad (1)$$

[26] This quantity is an approximation of the center of mass of the aerosol layer, that exactly coincides with the true center of mass if both composition and size distribution of the particles are constant with the altitude. This estimate of the center of mass gives us information about the altitude where the most relevant part of the aerosol load is located. As reported in Table 1, the core of the layer typically stays at about 3.5 km. In some cases a z_c higher than 4 km is observed, evidencing desert dust particles quickly lifted from the ground of the Sahara desert to high altitudes over the Mediterranean region.

[27] The high variability of the center of mass altitude is evident from Figure 2, where all values of z_c are reported together with the 70-day sliding average. The difference among the collected values is an expression of the natural variability of the Saharan dust intrusions process itself. However, the sliding average shows a clear seasonal dependence: During spring the altitude of the center of mass reaches its maximum of about 3.8 km, slowly decreasing in autumn down to 3 km. The same seasonal behavior is observed for the base of the desert dust layer. Its top, instead, has a maximum at the beginning of the summer with two minima, one at the end of spring and the other in autumn (not shown). The maximum top altitude of the desert dust layer observed during summer can be related to high convective conditions typical of this season, that can spread desert dust on a wider altitude range in summer than in winter. In the same period, the PBL height reaches its maximum of about 2.5 km a.s.l. [*Pandolfi et al.*, 2004], so that during summer the base of the desert dust layer and the PBL top are very close to each other. Therefore the intrusion of desert dust in the PBL more likely occurs during summer than in the rest of the year.

5. Optical Properties in the Desert Dust Layer

[28] Mean optical properties and vertically integrated optical properties are calculated within the identified aerosol layer. In particular, for each day of Saharan dust observation, the mean values of aerosol backscatter coefficient at 355 and 532 nm (β_{355}, β_{532}), and the aerosol extinction coefficient at 355 nm (α_{355}) are calculated within the desert dust layer. Aerosol integrated backscatter at 355 and 532 nm (IB_{355}, IB_{532}) and the aerosol optical depth (*OD*) are obtained by vertical integration within the desert dust layer of the vertical profiles of the corresponding optical parameters.

[29] Figure 3 reports the values of integrated backscatter at 532 nm observed in the period May 2000 to April 2003 and the corresponding 70-day sliding average. A mean IB_{532} of $(1.9 \pm 0.2) \times 10^{-3}$ sr^{-1} and a clear seasonal dependence

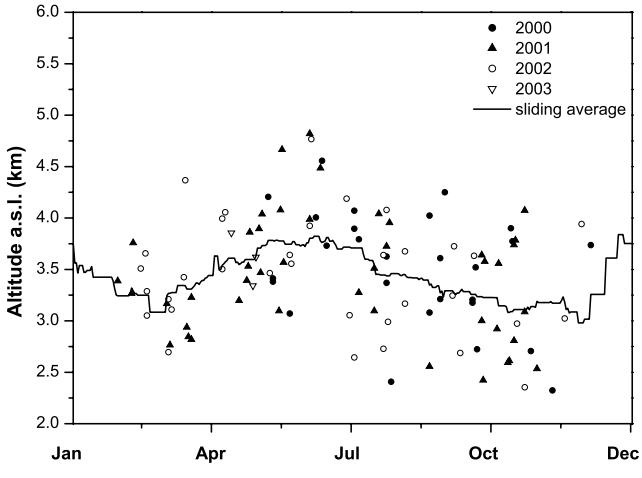

Figure 2. Annual cycle of the altitude of the center of mass of the desert dust layer (z_c). Solid circles, solid triangles, open circles, and open triangles represent the values observed in 2000, 2001, 2002 and 2003, respectively, while the solid line is the 70-day sliding average.

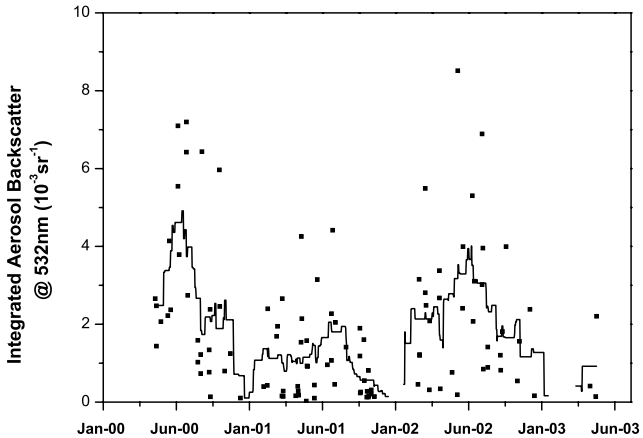

Figure 3. Temporal evolution of the integrated aerosol backscatter at 532 nm calculated in the individuated desert dust layer. The solid squares represent the observed values, while the solid line is the 70-day sliding average.

Table 2. Mean Value and Standard Deviation of the Aerosol Extinction Coefficient at 355 nm (α), of the Aerosol Backscatter Coefficient at 355 and 532 nm (β_{355}, β_{532}), of the Aerosol Optical Depth at 355 nm (*OD*), and of the Integrated Backscatter at Both Wavelengths (IB_{355}, IB_{532}) for the Whole Period of Observation (May 2000 to April 2003)[a]

		2000		2001			2002			2003
Parameter	Three Years	MJJA	SOND	JFMA	MJJA	SOND	JFMA	MJJA	SOND	JFMA
α_{355}, Mm^{-1}	76 ± 51	96	53	54	81	34	76	102	62	29
β_{355}, Im^{-1} sr^{-1}	1.0 ± 0.8	1.8	0.8	0.45	1.0	0.4	1.1	1.2	1.2	0.9
β_{532}, Im^{-1} sr^{-1}	0.54 ± 0.45	0.9	0.5	0.26	0.5	0.2	0.7	0.7	0.5	0.2
OD	0.13 ± 0.12	0.2	0.09	0.03	0.16	0.03	0.1	0.12	0.11	0.08
IB_{355}, 10^{-3} sr^{-1}	2.9 ± 2.5	5	3	1.3	3	0.9	2.9	3.5	3.7	4
IB_{532}, 10^{-3} sr^{-1}	1.9 ± 1.8	3	1.7	0.8	1.6	0.6	2.1	3.1	1.6	0.9
N_{obs}	112	18	10	13	18	14	13	15	8	3

[a]For each year, mean values of the same quantities are also reported for each 4-month period (e.g., May, June, July and August is indicated by MJJA). The number of observations (N_{obs}) is also reported for each one of the considered period.

with higher values in summer are observed. In the July–October 2000 and the March–July 2002 periods, very intense cases are observed: While more than 90% of measured values stay below 5×10^{-3} sr^{-1}, during this period higher IB_{532} values are often observed. Figure 3 clearly shows an IB_{532} measured in 2001 lower, on average, than in 2000 and 2002. The 70-day sliding average shows the absence in 2001 summer of extreme events, which were observed on the contrary in 2000 and 2002. In addition, a high occurrence of low intense events in 2001 is observed. In fact, in 3 years of measurements, in about 90% of the cases we observe an IB_{532} in the desert dust layer higher than 0.2×10^{-3} sr^{-1}. About 73% of these very low values are observed during 2001.

[30] Table 2 reports the mean and integrated values of the optical parameters calculated within the desert dust layer for the whole observation period (May 2000 to April 2003). For the 3-year averages, the standard deviation is also reported. A mean value within the desert dust layer of 76 Mm^{-1}, 1.0 Mm^{-1} sr^{-1} and 0.54 Mm^{-1} sr^{-1} is observed for the aerosol extinction at 355 nm, the aerosol backscatter at 355 nm and 532 nm, respectively. We have a mean optical depth at 355 nm of 0.13 and a mean integrated backscatter of 2.9×10^{-3} sr^{-1} and 1.9×10^{-3} sr^{-1} at 355 and 532 nm, respectively. A large standard deviation (up to a maximum of 95%) is observed for the optical parameters, as a result of the wide possibility of different scenario for the Saharan dust intrusion over Potenza. Optical properties are also influenced by dust composition and by the modification processes that occurred during the transport. Distributions for aerosol extinction at 355 nm, aerosol backscatter at 355 nm and 532 nm, and corresponding integrated quantities have a positive skewness, indicating a non Gaussian frequency distribution function, in accordance with the lognormal distribution found for aerosol properties [*Pandolfi et al.*, 2004; *Matthias et al.*, 2004b].

[31] For each year, the mean values of aerosol optical properties calculated in the desert dust layer for 4-month periods are also reported in Table 2. For the 2001 observations, the 4-month mean values for all the optical parameters are lower than the corresponding ones recorded during 2000, 2002 and 2003, confirming a lower dust load during the whole of 2001. The only exception is the aerosol extinction mean value of the first third of 2001 that is higher than the one observed in the same period of 2003, but we have to take into account that in the January–April 2003 period only few cases of dust intrusions are observed at IMAA. The highest values are typically observed in the second 4-month period of the year when the typical cyclone configuration favors the dust transport from the Sahara region to the Mediterranean area and a high number of Saharan dust events is also observed (Figure 1).

[32] The annual cycle of the dust load observed over Potenza in 3 years of measurements is reported in Figure 4 in terms of the aerosol optical depth at 355 nm calculated within the desert dust layer. Optical depth values show a large variability, ranging between a minimum of 0.001 and a maximum of 0.68. However, the 70-day sliding average clearly shows a strong seasonal behavior, slowly decreasing from 0.2 down to 0.005 between mid-August and the end of November. The same clear seasonal dependence, with the highest values observed in May–August period and with a lower desert aerosol load during autumn, has been observed for α_{355}, β_{355} and β_{532}, and for their corresponding integrated quantities. This is primarily due to the most intense transport, during late spring and summer, from the Sahara desert to the Mediterranean area because of cyclones that favor northward motions of air masses, in accordance with the large number of Saharan dust cases observed from May until July (Figure 1) and with satellite climatological studies [*Moulin et al.*, 1998].

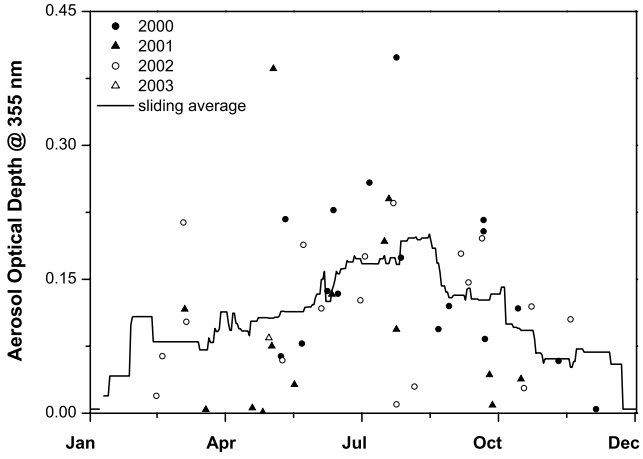

Figure 4. Annual cycle of the aerosol optical depth at 355 nm calculated inside the desert dust layer. Solid circles, solid triangles, open circles, and open triangles represent the values observed in 2000, 2001, 2002 and 2003, respectively, while the solid line is the 70-day sliding average.

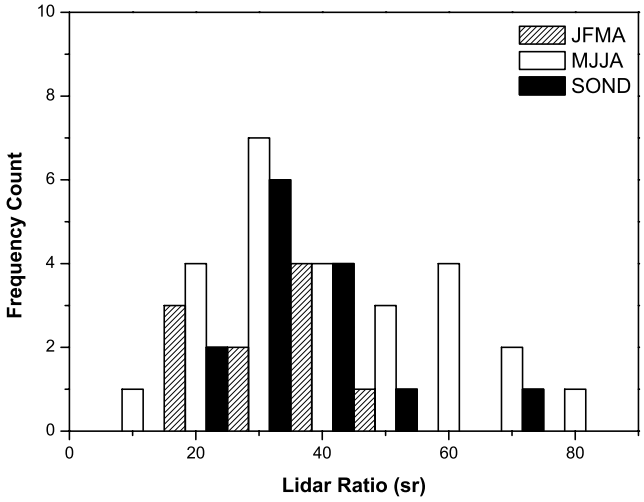

Figure 5. Frequency count distributions of the *LR* mean values at 355 nm calculated within the Saharan dust layer, for the three 4-month periods: January–April, May–August and September–December indicated as JFMA, MJJA and SOND, respectively.

[33] A suitable discussion is devoted to the lidar ratio (*LR*) and the backscatter Ångström exponent (δ). These two parameters depend only on microphysical properties of the aerosol, like dimension, chemical composition and shape, but not on the aerosol concentration. For each day of Saharan dust intrusion observed at our site, we calculated the weighted average for *LR* and δ inside the desert dust layer. Lidar ratio mean values at 355 nm range between 6 and 78 sr, with a mean value of 38 ± 15 sr, while the backscatter Ångström exponent has a mean of 1.5 ± 0.6 assuming values between −0.04 and 3.1. The lidar ratio mean value is in agreement with the theoretical value of about 45 sr calculated on the basis of the Mie theory [*Ackermann*, 1998]. For the backscatter Ångström exponent, small or even negative values are expected and were measured for dust aerosol [see, for example, *Mattis et al.*, 2002]. However, a mean value of 0.9, with values ranging from −1 to 3, has been observed for the backscatter Ångström exponent measured at the 355/532 nm within Saharan dust layer over Thessaloniki [*Balis et al.*, 2004]. This value seems to be caused mainly by the mixing of desert aerosol with local aerosols [*Balis et al.*, 2004].

[34] It is important to note that both the lidar ratio and the backscatter Ångström exponent widely vary as demonstrated by the large standard deviation of the mean and by the wide range of assumed values. This is true in particular for the backscatter Ångström exponent, in fact, our observations spread over the whole range of theoretical values, i.e., from −0.5 up to 3.

[35] For each day, we have considered the *LR* and δ mean values calculated in the desert dust layer, but it has to be taken into account that these parameters can strongly vary along the profile. A quantitative measure of the variability along the profile is obtained by the standard deviation from the mean, because it measures how much the observed values are spread inside the desert dust layer. On average, the variability along the desert dust layer is about 12 sr for the lidar ratio at 355 nm and about 1.7 for the backscatter Ångström exponent at 355/532 nm, showing an elevated dependence of these quantities on the altitude. The high variability of the intensive properties (*LR* and δ) can be ascribed to the variability of aerosol microphysical properties related to differences in the dust composition and to the modification processes occurring during the transport.

[36] Figure 5 reports the frequency count distributions of the *LR* mean values calculated within the Saharan dust layer, for the three 4-month periods. The centers of the distributions are not significantly different, but, *LR* mean values are more spread during the second 4-month period of the year than in the rest of the year. In particular, *LR* values higher than 50 sr are observed almost only during the May–August period. Moreover, this period is also characterized by the highest mean *LR* variability along the profile (14 sr against about 10 sr).

[37] In summer months, low values of the backscatter Ångström exponent are more frequent than in winter. However, no significant seasonal differences are observed in δ mean values, distribution width and in δ variability along the profile. This allows us to suppose that the dimension of transported dust, even if highly variable in both time and space, are on average the same and equally spread in the different periods of the year.

[38] The absence of a seasonal dependence for *LR* and δ mean values confirms that the seasonal behavior of extensive quantities, like the optical depth, is mainly due to the higher amount of Saharan dust transported across the Mediterranean Sea during the warm season than during the rest of the year. The larger variability observed for the lidar ratio in the May–August period can be exclusively ascribed to a more diverse aerosol type in terms of chemical composition and shape, probably related to differences between the aerosol transport mechanisms that occur in different periods of the year.

6. Dust Origin

[39] In order to investigate the origin of the Saharan dust transported over Potenza, a representative back trajectory for each Saharan dust observation at our site is identified. For each of these cases, we choose the trajectory closest in time to lidar measurements and related to the arrival pressure that best approximates the observed altitude of the desert dust layer center of mass. Combining this information with the TOMS aerosol index observations, we divide the Saharan dust observed over Potenza in three main source regions: the western Sahara (WS), the central Sahara (CS) and the eastern Sahara (ES). The geographic locations of these regions are reported in Figure 6 together with the typical path covered by the dust particles. The CS class is the most populated and contains about 65% of the total cases, while about 31% of the cases is related to the WS source region, and only in four cases over 3 years of measurements we observed Saharan dust coming from the east part of the Sahara.

[40] The monthly distribution of the number of intrusions divided in the individuated classes, reported in Figure 7, shows that dust intrusions observed over Potenza in the

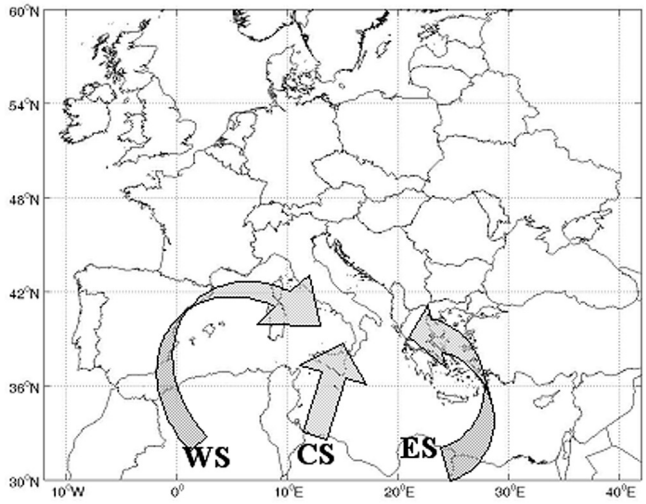

Figure 6. Source regions and typical path covered by the desert dust aerosol observed at IMAA during 3 years of measurements. From the combined use of DWD back trajectories and TOMS images we identify three main source regions: the western Sahara (WS), the central Sahara (CS) and the eastern Sahara (ES).

January–May period originated mainly in the central Sahara area. From Figure 7, it is also evident that desert dust coming from the western Sahara is typically observed at our site during summer and early autumn. Differences in the monthly behavior of the CS and WS classes are clearly related to the mean atmospheric conditions. In fact, during spring and early summer the formation of the Sharav cyclone is favored: It moves eastward starting from the south of the North African coast, crossing the Mediterranean between Libya and Egypt and reaching the central part of the Mediterranean Basin. In late summer, instead, air masses typically move from the northwestern African coast, turn around the Balearic Islands and point toward Italy [*Moulin et al.*, 1998]. However, both CS and WS cases are observed for almost each month of the year. In particular, during summer, CS and WS are the origin of a comparable number of Saharan dust intrusions over Potenza. This could explain the large variability of lidar ratio data collected in this period.

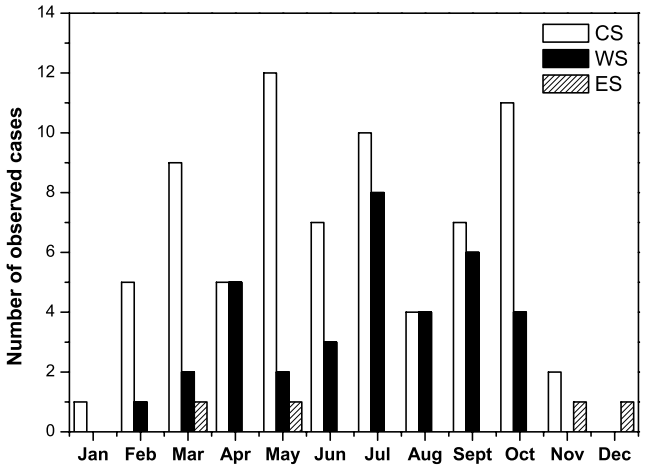

Figure 7. Monthly distributions of the number of intrusions divided for the source region of aerosol.

[41] Figure 8 reports mean aerosol backscatter profiles at 532 nm for each of the dust origin classes. A very low dust load is observed for ES in respect to WS and CS classes. Moreover, on average dust transported from the eastern Sahara are confined in the 3–5 km a.s.l. altitude range, whereas dust typically reaches altitudes as high as 7 km for cases falling in the two most populated classes. The CS mean aerosol backscatter decreases with the altitude with non–clearly defined aerosol layers, while two peaks at about 3.5 and 4.5 km a.s.l. seem to be present for the WS mean profile. However, the large standard deviation around the β mean profiles (about 50%) does not allow to infer a correlation between the Saharan dust layer vertical stratification and the desert dust origin. Figure 9 reports mean *LR* vertical profiles for Saharan dust coming from the central and the western part of Sahara. Both the two profiles vary around a mean value of about 40 sr and show higher values around 50 sr above 5 km, but in the central range of the desert dust layer, i.e., at about 3 km, the *LR* for dust coming

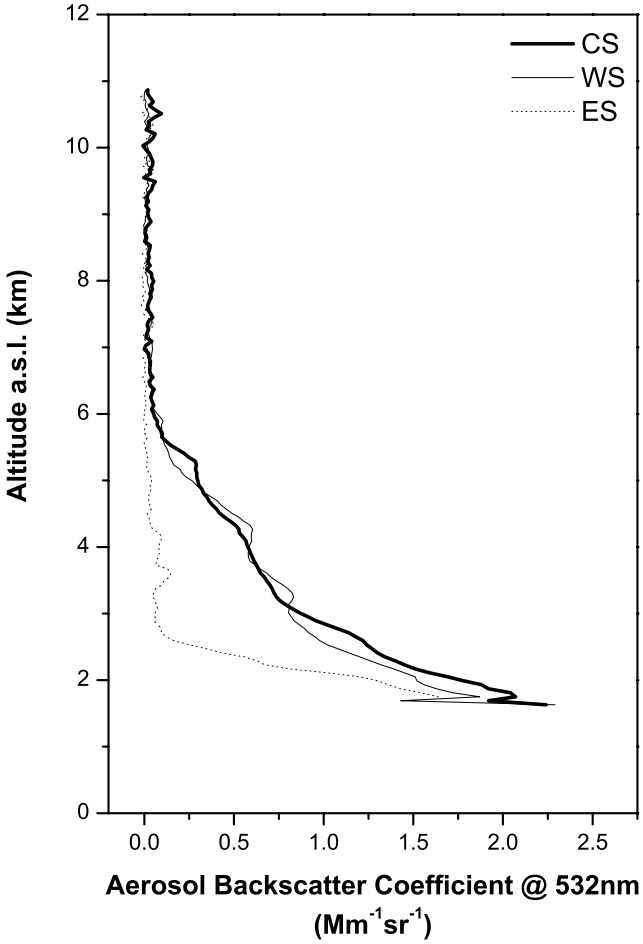

Figure 8. Mean aerosol backscatter profiles at 532 nm obtained averaging aerosol backscatter profiles belonging at each of the dust origin classes: Central Sahara is reported as the solid thick line, western Sahara is reported as the solid thin line and eastern Sahara is reported as the dotted line.

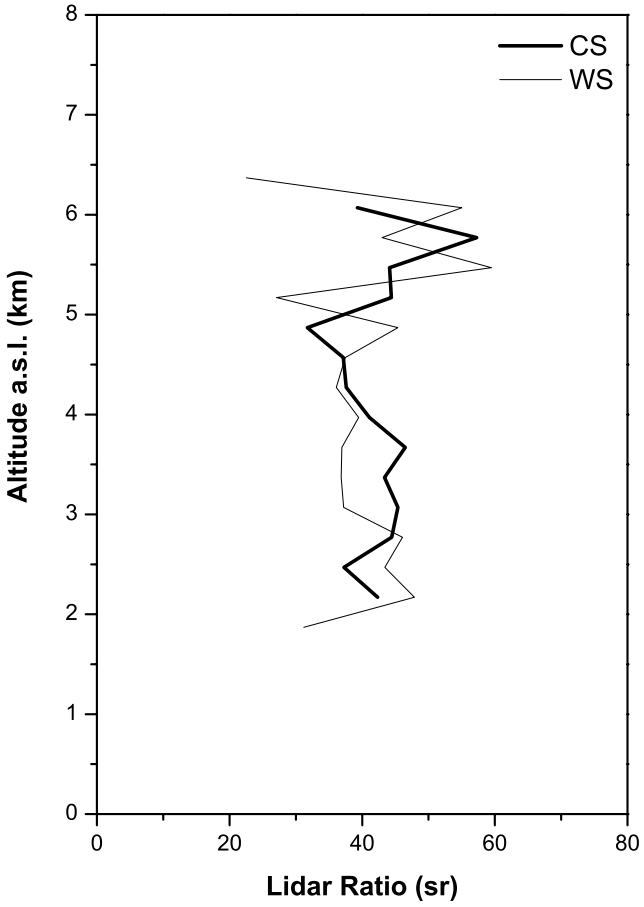

Figure 9. Mean *LR* vertical profiles for Saharan dust coming from the central and the western part of Sahara reported as solid thick line and solid thin line, respectively.

from the west of Sahara desert is lower than that related to CS area, about 36 sr against 45 sr. It could be supposed that the high variability observed in the lidar ratio value recorded in the May–August period (see Figure 5) is related to the transport of dust coming from the central and western part of Sahara. However, for both the two classes, the large standard deviation around the *LR* mean profile of about 22 sr is too high to draw a strong conclusion about the correlation between the origin of the dust and *LR* value.

7. Lidar Ratio

[42] In order to take into account the *LR* high variability observed along the desert dust layer, a more detailed analysis of the *LR* data is carried out considering all the *LR* data points collected within the individuated desert dust layer.

[43] Among the 112 Saharan dust observations, 50 lidar ratio profiles are collected. The relative low number of profiles is due to the low signal-to-noise ratio for the Raman signal that does not always allow a successful aerosol optical properties retrieval based on the combined Raman-elastic approach, especially in daytime conditions. Nevertheless, the total amount of about 400 *LR* data points is sufficiently high to carry out a detailed statistical analysis and provides the largest lidar ratio database for Saharan dust particles.

[44] Figure 10 reports the frequency count distribution of all *LR* data points collected within the Saharan dust layer (solid squares). *LR* ranges between 6 and 126 sr and this distribution is clearly more spread than that one reported in Figure 5 related only to the mean values inside the desert dust layer. Again, this is strictly related to the variability of the lidar ratio along the profile, that is intrinsically connected to the differences in size, shape and composition with the altitude. The distribution in Figure 10 clearly shows two peaks at about 20 and 40 sr, with the first one narrower than the second. A wider and more spread "bump" around 80 sr can be noticed. Besides experimental points, Figure 10 reports as a solid line the trimodal Gaussian distribution that best fits the experimental frequency count distribution, giving rise to a quadratic correlation coefficient $r^2 = 0.995$. The total distribution is the sum of three Gaussian distributions (dotted lines) centered around 21.9 ± 0.3 sr, 37.0 ± 1.6 sr and 57 ± 27 sr and characterized by a standard deviation of 4, 13 and 23 sr, respectively.

[45] The first mode centered around 21.9 sr is very narrow (small standard deviation and very low estimation error of the mode center), indicating a situation with high occurrence of *LR* values ranging between 18 and 26 sr and low variability. *LR* profiles almost constant with the altitude and characterized by low values are observed in 4 particular days of Saharan dust intrusion. The aerosol backscatter coefficient profiles at 532 nm for these 4 days are reported in Figure 11a. A high aerosol load is present at low altitude, showing that in these cases, desert dust has been transported from the desert over the Mediterranean Sea without a considerable lifting process. Therefore it is reasonable to suppose a strong mixture of desert dust and maritime aerosols. The frequency count distribution of *LR* values measured in these 4 days is reported in Figure 11b. The

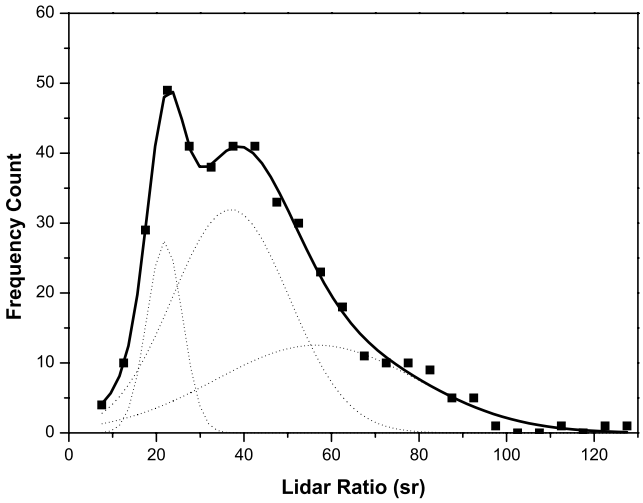

Figure 10. Frequency count distribution of all *LR* values at 355 nm collected within the Saharan dust layers (solid square). The solid line represents the three mode Gaussian distribution that best fits the experimental points: This curve is the sum of three single mode Gaussian distributions reported as dotted lines.

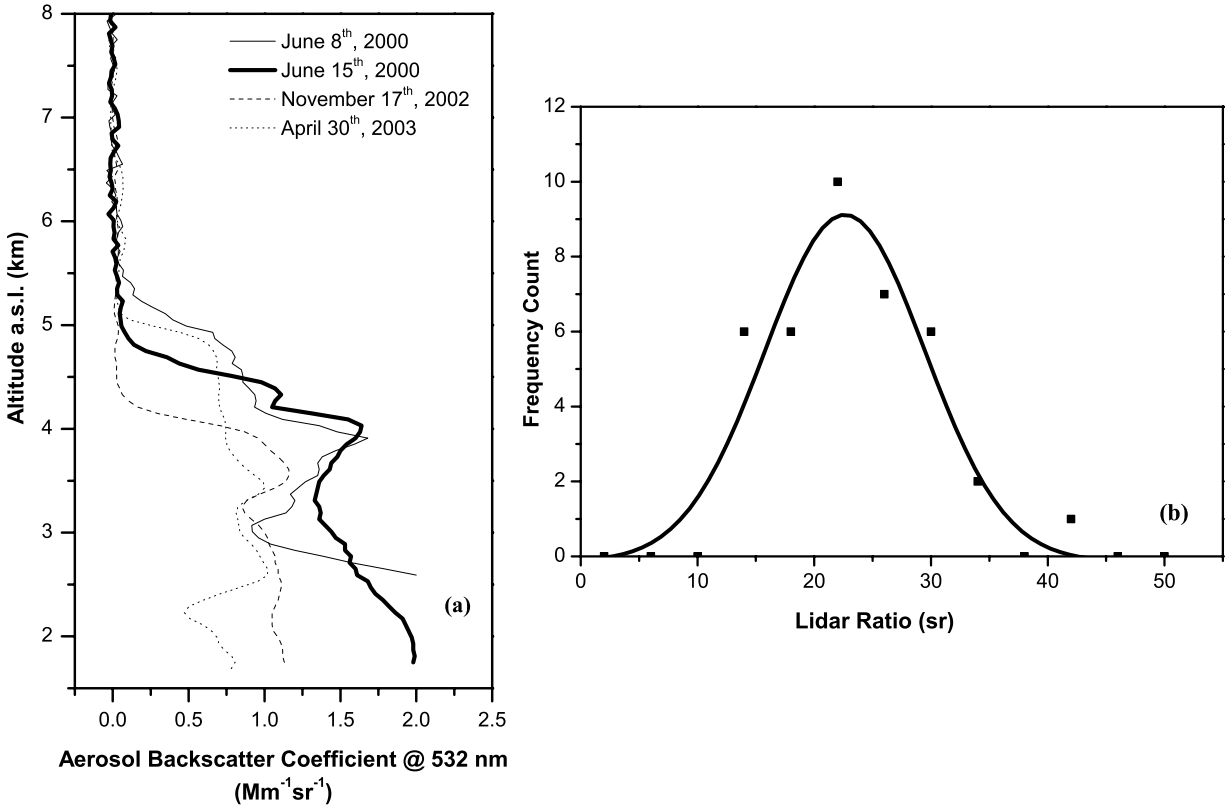

Figure 11. (a) Aerosol backscatter coefficient profiles at 532 nm for four cases in which *LR* assumes very low values within the individuated desert dust layer and (b) frequency count distribution of the corresponding *LR* values.

experimental points are well fitted ($r^2 = 0.92$) by a Gaussian distribution centered around 22.6 ± 0.6 sr and with a standard deviation of 6 sr.

[46] Figure 12 reports the remaining part of *LR* data (solid squares) as a function of the distance from the desert dust layer center of mass. In this plot, the high variability of this parameter is clearly evident. However, on average, the *LR* is almost constant with the altitude in a range extended between −0.5 and 0.5 km around z_c, as shown by the mean behavior of the *LR* as a function of the distance by z_c. Restricting our analysis to these data, a Gaussian distribution centered at 37.8 ± 1.3 sr is obtained as fitting curve of experimental points ($r^2 = 0.96$). This allows us to ascribe the central Gaussian distribution reported in Figure 10 to the core of the desert dust layer, where both contamination with the PBL and modification processes are less relevant. A *LR* mean value of about 38 sr is thus representative of what we can call ''pure Saharan dust,'' a value in perfect agreement with theoretical values reported in the literature [*Ackermann*, 1998]. On the other hand, cases of Saharan dust observations characterized by a mean *LR* at 355 nm of about 50 sr are reported [*Mattis et al.*, 2002; *De Tomasi et al.*, 2003]: The enhancement respect to the theoretical value is mainly ascribed to particle asphericity that strongly suppresses the backscatter. However, these studies deal with very intensive cases of Saharan dust transport, while in the present work a climatological study is carried out considering all, high as well as low, dust load cases. During the second 4-month period of the year, when strongest Saharan dust events occur, we observe a significant number of Saharan dust intrusions characterized by a mean lidar ratio higher than 50 sr (see Figure 5) and by a high frequency of low δ values. A possible explanation could be that in extreme events, the dust elevation mechanism involves more energy, therefore large particles can be lifted together with small ones and the mean particle size is higher than in cases involving less energy. Since nonspherical aerosol shape is more relevant as the particle dimension increases, during extreme events, *LR* values on average are higher than typically observed ones.

[47] Prior to this paper, the only further long-term climatological study of *LR* values for Saharan dust shows a mean value, measured in the eastern Mediterranean, of 51 sr with a standard deviation of 25 sr [*Balis et al.*, 2004], in fair agreement with our measurements. However, their high value can be attributed to different source region and traveled path of the observed dust, and to the crossing of polluted air over the eastern Mediterranean [*Lelieveld et al.*, 2002].

[48] The tails of the desert dust layer, i.e., closer to the PBL and at the top of the desert dust layer, are on average characterized by higher lidar ratio values. In addition, *LR* is highly variable as demonstrated by the error bars reported in Figure 12. This situation could be considered representative of the third mode retrieved by our all-data analysis. The mean value of about 60 sr can be related to the contamination with smaller, more absorptive particles that can be

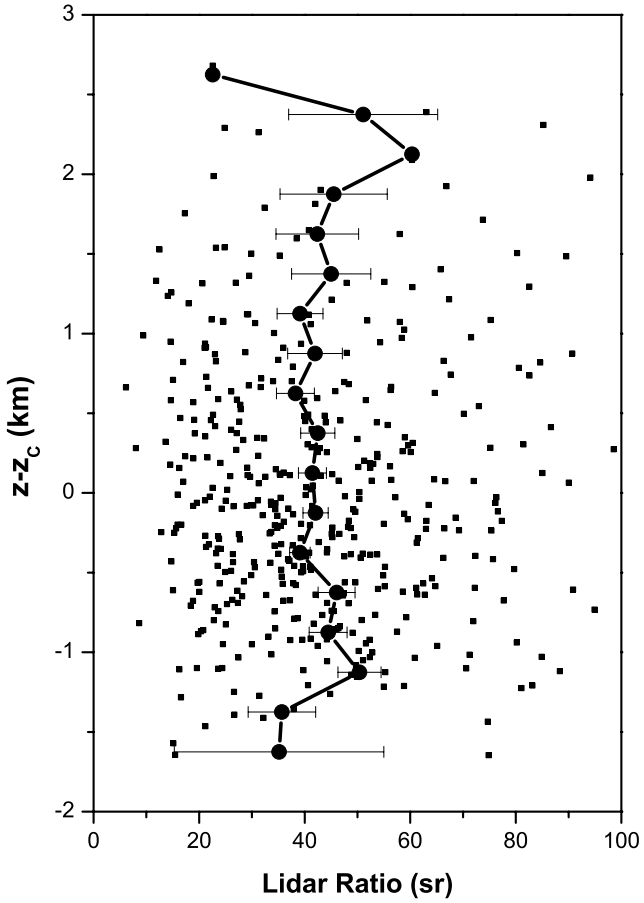

Figure 12. Lidar ratio values at 355 nm measured within the desert dust layer (solid squares) reported as a function of the distance from the desert dust layer center of mass (z-z_c), for all cases apart those of Figure 11. The solid line shows the mean behavior of the LR as a function of the distance from z_c, obtained calculating the averages (solid circles) of experimental values within interval ranges of 250 m. The error bars represent the variability within these intervals of altitude ranges.

found near the surface and also by the presence of smaller particles in the upper part of the desert dust layer.

8. Summary and Conclusions

[49] For the first time, a 3-year climatology of Saharan dust intrusion observations performed in the Mediterranean Basin is presented. The IMAA Raman/elastic lidar, located in Tito Scalo, in the central part of Mediterranean Sea, is part of EARLINET, the first lidar network for aerosol study on continental scale. At present, this is the longest climatological analysis of vertical profiles of Saharan dust optical properties and, in particular, it is the first climatological study of lidar ratio data for this kind of aerosol.

[50] Cases of Saharan dust intrusion have been selected among data systematically acquired within EARLINET, by means of air masses back trajectory analysis provided by DWD and with the support of TOMS aerosol index images. During May 2000 to April 2003 period, dust intrusions were observed in 112 days corresponding to about 1 day of desert dust intrusion every 10 days. In Potenza we observe aerosol coming from the Sahara desert every month of the year, with a major occurrence in the May–July period. In the same period we observe the highest desert dust aerosol load in terms of both optical depth and integrated backscatter. All the extensive aerosol optical parameters show a seasonal behavior with a pronounced maximum in the second 4-month period of the year and the same kind of behavior is observed for the top of the desert dust layer and for its thickness. On the contrary, the base and the center of mass of the desert dust layer have a maximum during spring and a minimum during summer.

[51] Aerosol layers related to dust intrusions were observed between 1.8 and 9 km a.s.l. with a mean center of mass altitude of about 3.5 km a.s.l. A mean optical depth of 0.13 at 355 nm is found for desert dust layers, reaching a maximum value of 0.68. The systematic observations performed at IMAA in the considered period show the presence of extreme events during 2000 and 2002, while on average the lowest values of integrated quantities were observed during 2001.

[52] Dust observed at Potenza has its main origin in central Sahara and reaches southern Italy almost directly, while in about 31% of cases dust has originated in western Sahara and passes over the Iberian Peninsula before pointing toward Italy. In only few cases the dust origin is in eastern Sahara. In summer, comparable occurrences of dust coming from western and central Sahara are observed, while dust intrusions observed over Potenza in the January–May period are originated mainly in the central Sahara.

[53] For the backscatter Ångström exponent, we obtained a mean value of 1.5 ± 0.6 and a very high variability (1.7) along the desert dust layer. No seasonal dependence and no origin dependence is observed for δ mean value and for its variability along the profile.

[54] A detailed analysis was performed in terms of the lidar ratio at 355 nm. Lidar ratio mean value along the profile of 38 ± 15 sr is in agreement with theoretical values of Saharan dust lidar ratio at 355 nm. Besides the high variability of lidar ratio desert dust layer mean value, a high variability of *LR* along the profile is also observed (12 sr on average), reflecting the natural variability of the dust generation, transport and modification processes. A more detailed analysis was performed considering not only the mean *LR* for each day of observation but all the *LR* values collected within the desert dust layer related to Saharan dust intrusion. At present, this is the most extended database of *LR* values, collected at one site, for Saharan dust aerosol. The frequency distribution of these points is well fitted by a trimodal gaussian distribution, centered around 22, 37 and 57 sr. Each of these values represents a different situation: A low lidar ratio around 22 sr is found for few cases of contamination between desert dust and maritime aerosols, in which high dust load transported at very low altitude. Lidar ratio values collected close to the desert dust layer center of mass are distributed around 37 sr, representing what we have called the ''pure Saharan dust.'' Finally a wide Gaussian distribution centered around 57 sr collects all the other situations in which the mixing between Saharan dust and free troposphere and PBL aerosols are relevant.

[55] These lidar ratio observations can be very useful for estimation of aerosol extinction from pure backscatter lidar,

widely used worldwide. In addition, these data provide an important instrument to improve and validate retrieval algorithms of future space-borne lidar, such as CALIPSO (Cloud-Aerosol Lidar and Infrared Pathfinder Satellite Observations), the first satellite-borne elastic lidar.

[56] **Acknowledgments.** The support of this work by the European Commission under grant EVRI-CT1999-40003 is gratefully acknowledged. The authors also thank the German Weather Service for the air mass back trajectory analysis and the NASA/GSFC for the EP/TOMS Aerosol Index images.

References

Ackermann, J. (1998), The extinction-to-backscatter ratio of tropospheric aerosol: A numerical study, *J. Atmos. Oceanic Technol.*, *15*, 1043–1050.

Andreae, M. O. (1995), Climate effects of changing atmospheric aerosol levels, in *World Survey of Climatology*, vol. 16, *Future Climate of the World*, edited by A. Henderson-Sellers, pp. 341–392, Elsevier, New York.

Ansmann, A., M. Riebesell, and C. Weitkamp (1990), Measurement of atmospheric aerosol extinction profiles with a Raman lidar, *Opt. Lett.*, *15*, 746–748.

Ansmann, A., M. Riebesell, U. Wandinger, C. Weitkamp, E. Voss, W. Lahmann, and W. Michaelis (1992), Combined Raman elastic-backscatter lidar for vertical profiling of moisture, aerosol extinction, backscatter and lidar ratio, *Appl. Phys. B*, *55*, 18–28.

Ansmann, A., F. Wagner, D. Müller, D. Althausen, A. Herber, W. von Hoyningen-Huene, and U. Wandinger (2002), European pollution outbreaks during ACE-2: Optical particle properties inferred from multiwavelength lidar and star-Sun photometry, *J. Geophys. Res.*, *107*(D15), 4259, doi:10.1029/2001JD001109.

Ansmann, A., et al. (2003), Long-range transport of Saharan dust to northern Europe: The 11–16 October 2001 outbreak observed with EARLINET, *J. Geophys. Res.*, *108*(D24), 4783, doi:10.1029/2003JD003757.

Balis, D. S., V. Amiridis, S. Nickovic, A. Papayannis, and C. Zerefos (2004), Optical properties of Saharan dust layers as detected by a Raman lidar at Thessaloniki, Greece, *Geophys. Res. Lett.*, *31*, L13104, doi:10.1029/2004GL019881.

Böckmann, C., et al. (2004), Aerosol lidar intercomparison in the framework of the EARLINET project. 2. Aerosol backscatter algorithms, *Appl. Opt.*, *43*, 977–989.

Bösenberg, J., et al. (2003), EARLINET: A European Aerosol Research Lidar Network to Establish an Aerosol Climatology, *MPI-Rep. 348*, Max-Planck-Inst., Hamburg, Germany.

d'Almeida, G. A. (1986), A model for Saharan dust transport, *J. Clim. Appl. Meteorol.*, *25*, 903–916.

d'Almeida, G. A., P. Koepke, and E. P. Shettle (1991), *Atmospheric Aerosol: Global Climatology and Radiative Characteristics*, A. Deepak, Hampton, Va.

De Tomasi, F., A. Blanco, and M. R. Perrone (2003), Raman lidar monitoring of extinction and backscattering of African dust layers and dust characterization, *Appl. Opt.*, *42*(9), 1699–1709.

di Sarra, A., M. Cacciani, P. Chamard, C. Cornwall, J. J. DeLuisi, T. Di Iorio, P. Disterhoft, G. Fiocco, D. Fuà, and F. Monteleone (2002), Effects of desert dust and ozone on the ultraviolet irradiance at the Mediterranean island of Lampedusa during PAUR II, *J. Geophys. Res.*, *107*(D18), 8135, doi:10.1029/2000JD000139.

Dulac, F., P. Buat-Menard, D. Sutton, D. Tanré, G. Bergametti, and M. Debois (1992), Assessment of the African airborne dust mass over the western Mediterranean Sea using Meteosat data, *J. Geophys. Res.*, *97*(D2), 2489–2506.

Evans, B. T. N. (1988), Sensitivity of the backscatter/extinction ratio to changes in aerosol properties: Implications for lidar, *Appl. Opt.*, *27*, 3299–3306.

Ferrare, R. A., S. H. Melfi, D. N. Whiteman, K. D. Evans, and R. Leifer (1998), Raman lidar measurements of aerosol extinction and backscattering: 1. Methods and comparison, *J. Geophys. Res.*, *103*(D16), 19,663–19,672.

Formenti, P., et al. (2001), Aerosol optical properties and large-scale transport of air masses: Observations at a coastal and a semiarid site in the eastern Mediterranean during summer 1998, *J. Geophys. Res.*, *106*(D9), 9807–9826.

Ginoux, P., and O. Torres (2003), Empirical TOMS index for dust aerosol: Applications to model validation and source characterization, *J. Geophys. Res.*, *108*(D17), 4534, doi:10.1029/2003JD003470.

Herman, J. R., P. K. Barthia, O. Torres, C. Hsu, C. Seftor, and E. Celarier (1997), Global distribution of UV-absorbing aerosols from Nimbus 7/TOMS data, *J. Geophys. Res.*, *102*(D14), 16,911–16,922.

Holben, B. N., et al. (1998), AERONET: A federated instrument network and data archive for aerosol characterization, *Remote Sens. Environ.*, *66*, 1–16.

Hsu, N. C., J. R. Herman, O. Torres, B. N. Holben, D. Tanre, T. F. Eck, A. Smirnov, B. Chatenet, and F. Lavenu (1999), Comparison of the TOMS aerosol index with Sun-photometer aerosol optical thickness: Results and applications, *J. Geophys. Res.*, *104*(D6), 6269–6279.

Husar, R. B., J. M. Prospero, and L. L. Stowe (1997), Characterization of tropospheric aerosols over the oceans with the NOAA advanced very high resolution radiometer optical thickness operational products, *J. Geophys. Res.*, *102*, 16,889–16,909.

Intergovernmental Panel on Climate Change (2001), *Climate Change 2001: The Scientific Basis*, edited by J. T. Houghton et al., Cambridge Univ. Press, New York.

Kaufman, Y. J., D. Tanré, and O. Boucher (2002), A satellite view of aerosols in the climate system, *Nature*, *419*, 215–223.

La Fontaine, C. V., et al. (1990), Airstream regions of North Africa and the Mediterranean, *J. Clim.*, *5*, 646–656.

Lelieveld, J., et al. (2002), Global air pollution crossroads over the Mediterranean, *Science*, *298*, 794–799.

Lundholm, B. (1979), Ecology and dust transport, in *Saharan Dust, Mobilization, Transport, Deposition, SCOPE 14*, edited by C. Morales, pp. 61–68, John Wiley, Hoboken. N. J.

Marticorena, B., and G. Bergametti (1996), Two-year simulations of seasonal and interannual changes of the Saharan dust emissions, *Geophys. Res. Lett.*, *23*(15), 1921–1924.

Marticorena, B., G. Bergametti, B. Aumont, Y. Callot, C. N'Doumé, and M. Legrand (1997), Modeling the atmospheric dust cycle: 2. Simulation of Saharan dust sources, *J. Geophys. Res.*, *102*(D4), 4387–4404.

Matthias, V., et al. (2004a), Aerosol lidar intercomparison in the framework of the EARLINET project. 1. Instruments, *Appl. Opt.*, *43*, 961–976.

Matthias, V., et al. (2004b), The vertical aerosol distribution over Europe: Statistical analysis of Raman lidar data from 10 EARLINET stations, *J. Geophys. Res.*, *109*, D18201, doi:10.1029/2004JD004638.

Mattis, I., A. Ansmann, D. Müller, U. Wandinger, and D. Althausen (2002), Dual-wavelength Raman lidar observations of the extinction-to-backscatter ratio of Saharan dust, *Geophys. Res. Lett.*, *29*(9), 1306, doi:10.1029/2002GL014721.

Mattis, I., A. Ansmann, U. Wandinger, and D. Müller (2003), Unexpectedly high aerosol load in the free troposphere over central Europe in spring/summer 2003, *Geophys. Res. Lett.*, *30*(22), 2178, doi:10.1029/2003GL018442.

Mishchenko, M. I., L. D. Travis, R. A. Kahn, and R. A. West (1997), Modeling phase functions for dustlike tropospheric aerosols using a shape mixture of randomly oriented polydisperse spheroids, *J. Geophys. Res.*, *102*(D14), 16,831–16,847.

Moulin, C., F. Dulac, C. E. Lambert, P. Chazette, I. Jankowiak, B. Chatenet, and F. Lavenu (1997), Long-term daily monitoring of Saharan dust load over ocean using Meteosat ISCCP-B2: 2. Accuracy of the method and validation using Sun photometer measurements, *J. Geophys. Res.*, *102*(D14), 16,959–16,969.

Moulin, C., et al. (1998), Satellite climatology of African dust transport in the Mediterranean atmosphere, *J. Geophys. Res.*, *103*(D11), 13,137–13,144.

Müller, D., U. Wandinger, D. Althausen, and M. Fiebig (2001), Comprehensive particle characterization from three-wavelength Raman-lidar observations: case study, *Appl. Opt.*, *40*(27), 4863–4869.

Murayama, T., D. Müller, K. Wada, A. Shimizu, M. Sekiguchi, and T. Tsukamoto (2004), Characterization of Asian dust and Siberian smoke with multiwavelength Raman lidar over Tokyo, Japan in spring 2003, *Geophys. Res. Lett.*, *31*, L23103, doi:10.1029/2004GL021105.

Pace, G., A. di Sarra, D. Meloni, S. Piacentino, and P. Chamard (2005), Aerosol optical properties at Lampedusa (central Mediterranean)—1. Influence of transport and identification of different aerosol types, *Atmos. Chem. Phys. Disc.*, *5*, 1–41.

Pandolfi, M., A. Amodeo, C. Cornacchia, L. Mona, and G. Pappalardo (2004), Three years of Raman lidar measurements of tropospheric aerosol over Potenza in the framework of EARLINET, in *22nd International Laser Radar Conference, 12–16 July 2004 Matera, Italy*, edited by G. Pappalardo and A. Amodeo, *Eur. Space Agency Spec. Publ. ESA SP-561*, *2*, 853–856.

Papayannis, A., et al. (2004), Saharan dust outbreaks towards Europe: 3 years of systematic observations by the European lidar network in the frame of the EARLINET project (2000–2003), in *22nd International Laser Radar Conference, 12–16 July 2004 Matera, Italy*, edited by G. Pappalardo and A. Amodeo, *Eur. Space Agency Spec. Publ. ESA SP-561*, *2*, 845–848.

Papayannis, A., D. Balis, V. Amiridis, G. Chourdakis, G. Tsaknakis, C. Zerefos, A. D. A. Castanho, S. Nickovic, S. Kazadzis, and J. Grabowski (2005), Measurements of Saharan dust aerosols over the eastern Mediter-

ranean using elastic backscatter-Raman lidar, spectrophotometric and satellite observations in the frame of the EARLINET project, *Atmos. Chem. Phys.*, *5*, 2065–2076.

Pappalardo, G., A. Amodeo, S. Amoruso, L. Mona, M. Pandolfi, and V. Cuomo (2003), One year of tropospheric lidar measurements of aerosol extinction and backscatter, *Ann. Geophys.*, *46*, 401–413.

Pappalardo, G., et al. (2004a), Aerosol lidar intercomparison in the framework of the EARLINET project. 3. Raman lidar algorithm for aerosol extinction, backscatter and lidar ratio, *Appl. Opt.*, *43*, 5370–5385.

Pappalardo, G., A. Amodeo, C. Cornacchia, L. Mona, and M. Pandolfi (2004b), Systematic tropospheric aerosol lidar observations, *Proc. SPIE Int. Soc. Opt. Eng.*, *5547*, 57–67.

Pappalardo, G., A. Amodeo, L. Mona, M. Pandolfi, N. Pergola, and V. Cuomo (2004c), Raman lidar observations of aerosol emitted during the 2002 Etna eruption, *Geophys. Res. Lett.*, *31*, L05120, doi:10.1029/2003GL019073.

Prospero, J. M. (1999), Long-range transport of mineral dust in the global atmosphere: Impact of African dust on the environment of the southeastern United States, *Proc. Natl. Acad. Sci. U.S.A.*, *96*, 3396–3403.

Prospero, J. M., P. Ginoux, O. Torres, S. E. Nicholson, and T. E. Gill (2002), Environmental characterization of global sources of atmospheric soil dust identified with the Nimbus 7 Total Ozone Mapping Spectrometer (TOMS) absorbing aerosol products, *Rev. Geophys.*, *40*(1), 1002, doi:10.1029/2000RG000095.

Pruppacher, H. R., and J. D. Klett (1997), *Microphysics of Clouds and Precipitation*, Springer, New York.

Robock, A. (2000), Volcanic eruptions and climate, *Rev. Geophys.*, *38*, 191–219.

Rosenfeld, D. (2000), Suppression of rain and snow by urban and industrial air pollution, *Science*, *287*, 1793–1796.

Sasano, Y., and E. V. Browell (1989), Light scattering characteristics of various aerosol types derived from multiple wavelength lidar observations, *Appl. Opt.*, *28*, 1670–1679.

Sassen, K., P. J. DeMott, J. M. Prospero, and M. R. Poellot (2003), Saharan dust storms and indirect effects on clouds: CRYSTAL-FACE results, *Geophys. Res. Lett.*, *30*(12), 1633, doi:10.1029/2003GL017371.

Sokolik, I. N., and O. B. Toon (1996), Direct radiative forcing by anthropogenic airborne mineral aerosols, *Nature*, *381*, 681–683.

Sokolik, I. N., D. M. Winker, G. Bergametti, D. A. Gillette, G. Carnichael, Y. J. Kaufman, L. Gomes, L. Schuetz, and J. E. Penner (2001), Introduction to special section: Outstanding problems in quantifying the radiative impacts of mineral dust, *J. Geophys. Res.*, *106*, 18,015–18,027.

Stohl, A. (1998), Computation, accuracy and applications of trajectories—A review and bibliography, *Atmos. Environ.*, *32*(6), 947–966.

Veselovskii, I., A. Kolgotin, V. Griaznov, D. Müller, U. Wandinger, and D. N. Whiteman (2002), Inversion with regularization for the retrieval of tropospheric aerosol parameters from multiwavelength lidar sounding, *Appl. Opt.*, *41*(18), 3685–3699.

Wandinger, U., and A. Ansmann (2002), Experimental determination of the lidar overlap profile with Raman lidar, *Appl Opt.*, *41*, 511–514.

Whiteman, D. N. (2003a), Examination of the traditional Raman lidar technique. I. Evaluating the temperature-dependent lidar equations, *Appl. Opt.*, *42*(15), 2571–2592.

Whiteman, D. N. (2003b), Examination of the traditional Raman lidar technique. II. Evaluating the ratios for water vapor and aerosols, *Appl. Opt.*, *42*(15), 2593–2608.

A. Amodeo, L. Mona, M. Pandolfi, and G. Pappalardo, Istituto di Metodologie per l'Analisi Ambientale, Consiglio Nazionale delle Ricerche, I-85050 Tito Scalo, Italy. (mona@imaa.cnr.it)